JACS
JOURNAL OF THE AMERICAN CHEMICAL SOCIETY
pubs.acs.org/JACS
Communication

Synthesis of the Candidate Topological Compound Ni_3Pb_2

Alexandra D. Tamerius,[⊥] Alison B. Altman,[⊥] Michael J. Waters, Eric A. Riesel, Christos D. Malliakas, Matthew L. Whitaker, Tony Yu, Gilberto Fabbris, Yue Meng, Daniel Haskel, Yanbin Wang, Steven D. Jacobsen, James M. Rondinelli,* and Danna E. Freedman*

Cite This: https://doi.org/10.1021/jacs.2c03485
Read Online
ACCESS | Metrics & More | Article Recommendations | Supporting Information

ABSTRACT: Spin−orbit coupling enables the realization of topologically nontrivial ground states. As spin−orbit coupling increases with increasing atomic number, compounds featuring heavy elements such as lead offer a pathway toward creating new topologically nontrivial materials. By employing a high-pressure flux synthesis method, we synthesized single crystals of Ni_3Pb_2, the first structurally characterized bulk binary phase in the Ni−Pb system. Combining experimental and theoretical techniques, we examined structure and bonding in Ni_3Pb_2, revealing the impact of chemical substitutions on electronic structure features of importance for controlling topological behavior. From these results, we determined that Ni_3Pb_2 completes a series of structurally related transition-metal-heavy main group intermetallic materials that exhibit diverse electronic structures, opening a platform for synthetically tunable topologically nontrivial materials.

Over the past decade, the field of topological materials grew at an explosive pace, fundamentally reshaping our depiction of solid-state systems.[1−5] Topologically nontrivial materials host band structures that enforce transport along specific paths, for example through spin-momentum locking and surface currents.[6−8] This phenomenon offers the potential to protect electron transport from sources of noise[9,10] with spintronic[11,12] and fault-tolerant quantum computing applications.[13−16] Recent computational studies demonstrate that topologically nontrivial classifiers are shared by ∼30% of known materials.[17] However, progressing from the classification of band structures to the application of useful transport properties, dependent on the overall electronic structure of each system, remains a key hurdle in the field. Amelioration of this challenge requires the creation of topologically nontrivial single crystal compounds, where the response of the material's band structure to chemical changes can be predicted, designed, and harnessed.[18]

Topological character is defined by the symmetry of the electronic wave functions of a material, reflecting two chemically intertwined effects: the real space symmetry of the system, as well as the interaction and identity of the atoms that comprise it.[19−21] Together they determine the band dispersions and crossings as well as the position of the Fermi energy relative to features of interest. To uncover the principles underpinning topological behavior, we pursued an approach to maintain physical structure and symmetry while introducing degrees of chemical freedom, allowing for minute adjustments. Targeting binary phases, whereby doping with a third element would be synthetically accessible, promises the requisite combination of precise chemical tunability and structural control.

High-pressure techniques are powerful tools for synthesizing new binary intermetallic materials, as they effectively add another axis to temperature−composition phase space.[22−26] Pressure also changes chemical heuristics,[27] promoting reactivity of high atomic number elements that introduce large amounts of spin−orbit coupling (SOC),[28−31] a key component in creating the targeted topological band structures motifs of interest.[32,33] To search for new topologically nontrivial phases, we explored the Ni−Pb system in which no bulk and thermodynamically stable materials are known, yet a report of bimetallic films accessed via vapor deposition suggests metastable reactivity.[34−36] Since Pb is the heaviest element stable to radioactive decay, we anticipated a strong SOC contribution to the band structure from Pb.[37−39] Employing high-pressure techniques, we synthesized and recovered the new Ni−Pb binary intermetallic phase, Ni_3Pb_2, elucidating its structure. Computational comparison of Ni_3Pb_2 with chemically related systems reveals its flexible topologically nontrivial character.

To synthesize Ni_3Pb_2, we performed high-pressure reactions using a Kawai-type multianvil press (MAP). We pressurized a pellet composed of a mixture of Ni and Pb to 8.4(1) GPa (see Supporting Information (SI) for details, Figure S4),[40] monitoring the reaction progress using synchrotron powder X-ray diffraction (PXRD) (λ = 0.1923 Å, MAXPD Endstation at NSLS-II, 28-ID-2-D). While heating the mixture to ∼1123 K, we observed the formation of new diffraction peaks corresponding to a pseudohexagonal structure[41] (Figure 1 and SI). Notably, decompression experiments revealed that the material persists to ambient conditions (Figure S9).

Received: March 31, 2022

https://doi.org/10.1021/jacs.2c03485
J. Am. Chem. Soc. XXXX, XXX, XXX−XXX

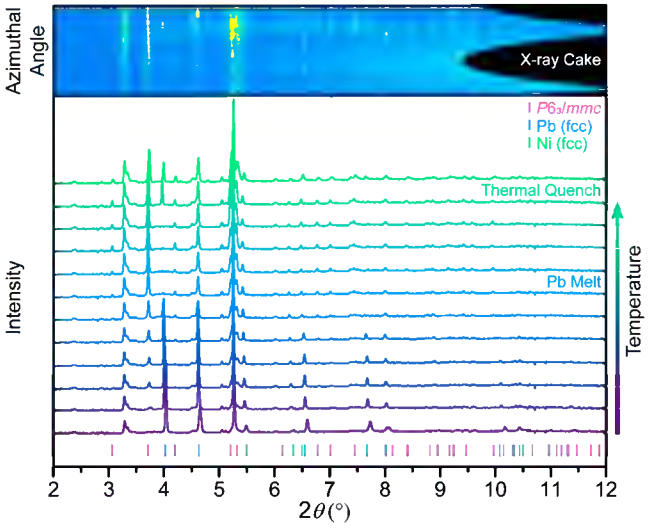

Figure 1. *In situ* PXRD data collected while heating a mixture of elemental nickel and lead at 8.4(1) GPa (λ = 0.1923 Å). The PXRD patterns (bottom) show the structural evolution with increasing temperature up to and beyond the lead melt (~1123 K) as well as the ambient temperature data (green). The $P6_3/mmc$ ticks (pink) correspond to the new phase. The unrolled cake image (top) shows a slice of the 2D PXRD pattern collected at ambient temperature.

Using the conditions established during the *in situ* studies, we scaled up the reaction (Figure S5) (APS, 13-ID-D).[40] As a consequence of the formation of a lead flux at high pressure, we found that the recovered samples consisted of high-quality crystallites amenable to structural characterization. Ambient pressure single crystal X-ray diffraction data revealed that Ni_3Pb_2 crystallizes in the $P2_1(\alpha 0\gamma)0$ superspace group with unit cell constants of a = 4.1705(2) Å, b = 5.2881(3) Å, c = 4.1848(2) Å, and β = 119.881(4)°, $q = 0.5a^* + 0.25c^*$ (Figure 2 center; see SI for details). It is a commensurately modulated member of the B8-type structure family and can be reduced to an orthorhombic cell setting, isostructural to the known *Pnma* superstructures of Ni_3Sn_2 and Co_3Sn_2.[42] Structural modulations exist presumably due to long-range ordering between Ni atoms and vacancies.

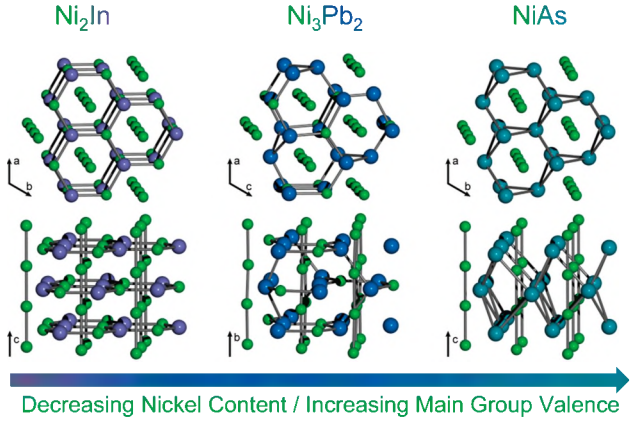

Figure 2. Comparison of the Ni_3Pb_2 crystal structure (generated from a supercell in the *P*1 space group, a = 8.3410(2) Å, b = 5.2881(3) Å, c = 16.7392(2) Å, α = 90, β = 119.881(4), γ = 90) with the NiAs and Ni_2In structures. Ni, In, Pb, and As are represented by green, purple, blue, and teal, respectively. The structures differ by the decrease in the occupancy of the Ni2 site from 1 → 0 across the series.

Many compounds within the B8-type family possess a nontrivial topological $\mathbb{Z}$-valued invariant, recommending this example for further investigation.[43] Structurally, Ni_3Pb_2 can be described as an intermediate between NiAs ($B8_1$) and Ni_2In ($B8_2$) if we consider the occupancy of the Ni atoms (Figure 2). All three structures share several features. They have chains of Ni atoms (Ni1 site) running along the *c*-axis in the $P6_3/mmc$ cell (*b*-axis in the $P2_1(\alpha 0\gamma)0$ cell) and triangular layers of main-group atoms perpendicular to the Ni chains where each layer is shifted by half a unit cell. Beyond the NiAs and isostructural NiSb structure, Ni_2In has a second Ni site (Ni2 site) that sits in the holes within the main group layers creating hexagonal layers of alternating Ni and main group atoms. In the Ni_3Pb_2 structure, this Ni2 site is half occupied. The overall similarities of these structures outside of the occupancy of a single type of site promise chemical tunability while maintaining overall structural motifs.

However, precise symmetry descriptions are crucial for evaluating topological character. Single crystal X-ray diffraction experiments revealed that the void space introduced by the Ni2 half-occupancy results in a distortion away from hexagonal symmetry shared by the NiAs and Ni_2In examples. This distortion to lower symmetry is observed in the isostructural Ni_3Sn_2 phase,[37] suggesting that the malleability of the hexagonal symmetry is generalizable for this stoichiometry of B8 compounds. The precise atomic positions revealed by our structure solution allows for visualization of the atom-specific interactions that drive the symmetry lowering, seen as undulations in the chains of Ni1. We posit these interactions serve to optimize Ni−Pb bond distances and stabilize Ni−Ni bonding interactions, differentiating the crystal symmetry in this series of materials based on local interactions. Further, many of the Ni−Pb distances (2.504(5)−2.9(1) Å) fall within the sum of the metallic radii (Ni, 1.244 Å; Pb, 1.746 Å).[44] The persistence of these interactions, despite ~3% changes in radius ratios of these elements over the pressure range explored,[45,46] suggest a sufficient energy barrier to decomposition enabling its persistence at ambient pressure. Together, these observations indicate the power of high-pressure synthesis to expand chemical control over structure in this class of materials.

To interrogate the potential topological properties of Ni_3Pb_2, we performed electronic structure calculations on the relaxed Ni_3Pb_2 structure at ambient pressure (Figure 3 and SI for details).[47] Examination of the band structure showed that the Ni *d* orbitals comprise the majority of bands near the Fermi level, as is expected for intermetallic phases with *sd*- and *p*-band metals. Below the Fermi energy, Pb *p* orbitals also contribute to the structure, suggesting orbital overlap that enables Ni-*d*−Pb-*p* bonding. Two-band crossings are observed at the Fermi energy, one at the S-point and one along the Γ−X trajectory with potential topological importance. By combining band structure calculations with elementary band representations and compatibility relations,[17,48] we determined that the topological classification describing the highest energy occupied bands in Ni_3Pb_2 is $\mathbb{Z}_4$ = 3, confirming that Ni_3Pb_2 is a candidate topologically nontrivial material. This topological index points to the presence of Dirac or Weyl nodes depending on the inversion and time reversal symmetry of the system.[49−53] Specifically, Ni_3Pb_2 exhibits avoided crossing that may engender Dirac nodes at interfaces that support unusual charge and spin transport properties.

https://doi.org/10.1021/jacs.2c03485
J. Am. Chem. Soc. XXXX, XXX, XXX−XXX

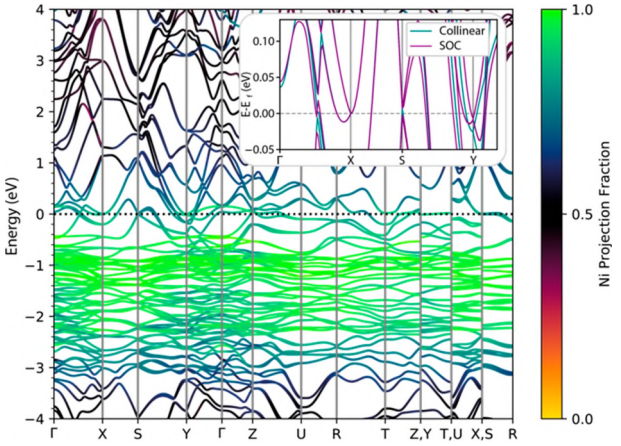

Figure 3. Band structure of Ni_3Pb_2 at ambient pressure where the bands are color coded to indicate the contribution of Ni electrons to each band. The inset highlights the band crossings near the Fermi level with (purple) and without (green) SOC.

Crucially, this nontrivial topological classifier differs from the NiAs and Ni_2In systems, which are predicted to have enforced semimetal character.[54−57] In comparison, at the S point of the band structure for Ni_3Pb_2 we observe a gap that introduces topological insulating character. To explore the origin of this gap, we made a series of comparisons. First, we observed that when SOC is not included in our calculation, this gap of ∼10 meV disappears (Figure S47). Similarly, examining the previously determined topological character of Ni_3Sn_2 reveals a similar phenomenon, although the gap at the S point is significantly smaller (<1 meV), further reflecting the importance of SOC in tuning topological character.[58] Complementarily, we computationally enforced a hexagonal primitive cell in Ni_3Pb_2 equivalent to having ordered half-occupied Ni2 sites in the $P6_3/mmc$ primitive cell of Ni_2In, resulting in a $P\bar{6}m2$ structure in which topological semimetal character is recovered (Figures S49 and S50). Thus, the nature of the topologically protected crossing at the S point reflects both the overall symmetry of the Ni2 site occupations as well as the amount of SOC engendered by the main group atom.

Controlling the extent of site occupancy in a material can pose a synthetic challenge. However, in B8-type Ni−main group phases, the main group element identity is known to determine the amount of Ni incorporated, which, in turn, determines the symmetry of the structure.[59] Namely, the amount of Ni incorporated decreases as the valence electron count on the main group element increases, such that main group elements requiring more electrons to achieve full orbital configurations incorporate more Ni into their structure. Indeed, Ni_3Pb_2 falls within this trend. One physical manifestation of this model is the expected charge transfer from the Ni center to the Pb, compensating for unfilled p-band electronic states. Examination of the electron density around each metal using X-ray absorption spectroscopy (XAS) revealed a shift of the Pb L_3-edge (13030(2) eV) to lower energy than the reference (13035 eV), and the Ni K-edge (8339(2) eV) to higher energy than the reference (8333 eV).[60] These data are consistent with XAS spectra for known Ni−main group B8-type compounds[61−65] as well as calculated projected charges (Table S32), confirming that there is a partial negative charge transfer from the Ni to the main group element. Thus, the role of the main group metal is twofold: its atomic number directly determines the amount of band mixing in the avoided crossings and its electron count indirectly influences the overall symmetry of the material based on the amount of Ni incorporated into the structure, creating a tractable synthetic handle to control topology.

In parallel, we also explored computationally the electronic structure of the hypothetical Co_3Pb_2 material inspired by the known isostructural Co_3Sn_2 phase. Although we were not able to synthesize any phase in this system under analogous conditions in a diamond anvil cell (up to 16 GPa, ∼1123 K), this is consistent with calculations that show its enthalpy of formation only becomes negative under higher pressure conditions (Figures S52−S56). Notably, electronic structure calculations revealed that a magnetic ground state is predicted, suggesting an additional handle for expanding topological behavior in systems without time-reversal symmetry. However, by enforcing nonmagnetic ordering in the predicted Co_3Pb_2 phase to allow for direct comparison with Ni_3Pb_2, we found that its hypothetical density of states is well-described within a rigid-band approximation. The Fermi level is shifted by ∼+0.75 eV relative to that in Ni_3Pb_2. This result combined with the analogous chemistry of Co_3Sn_2 suggests that transition metal identity provides another parameter for tuning topological properties, determining the energy of the Fermi level relative to topological electronic states while maintaining the overall symmetry. Explorations of chemical substitution through alloying at both the Ni and the main group metal site are of interest for future studies.

Our high-pressure discovery of Ni_3Pb_2 completes a series of B8-type compounds to reveal a chemical phase space in which overall structural motifs are maintained while electronic structure factors relevant for topology are tuned. This approach is promising for the creation of new families of flexible topologically nontrivial materials. Future studies will focus on doping this material to tune its Fermi energy and extending this conceptual approach to create new topologically nontrivial materials.

■ ASSOCIATED CONTENT

Supporting Information

The Supporting Information is available free of charge at https://pubs.acs.org/doi/10.1021/jacs.2c03485.

Additional synthesis and data analysis details, crystallographic refinements and structure solutions, and details for electronic structure calculations. (PDF)

Accession Codes

CCDC 2163166 contains the supplementary crystallographic data for this paper. These data can be obtained free of charge via www.ccdc.cam.ac.uk/data_request/cif, or by emailing data_request@ccdc.cam.ac.uk, or by contacting The Cambridge Crystallographic Data Centre, 12 Union Road, Cambridge CB2 1EZ, UK; fax: +44 1223 336033.

■ AUTHOR INFORMATION

Corresponding Authors

James M. Rondinelli − *Department of Material Science and Engineering, Northwestern University, Evanston, Illinois 60208, United States;* orcid.org/0000-0003-0508-2175; Email: jrondinelli@northwestern.edu

Danna E. Freedman − *Department of Chemistry, Massachusetts Institute of Technology, Cambridge,*

https://doi.org/10.1021/jacs.2c03485
J. Am. Chem. Soc. XXXX, XXX, XXX−XXX

Massachusetts 02142, United States; orcid.org/0000-0002-2579-8835; Email: danna@mit.edu

Authors

Alexandra D. Tamerius − *Department of Chemistry and Physical Sciences, Marian University, Indianapolis, Indiana 46222, United States; Department of Chemistry, Northwestern University, Evanston, Illinois 60208, United States*

Alison B. Altman − *Department of Chemistry, Northwestern University, Evanston, Illinois 60208, United States; Department of Chemistry, Massachusetts Institute of Technology, Cambridge, Massachusetts 02142, United States;* orcid.org/0000-0002-4975-5004

Michael J. Waters − *Department of Material Science and Engineering, Northwestern University, Evanston, Illinois 60208, United States;* orcid.org/0000-0001-6425-4331

Eric A. Riesel − *Department of Chemistry, Massachusetts Institute of Technology, Cambridge, Massachusetts 02142, United States*

Christos D. Malliakas − *Department of Chemistry, Northwestern University, Evanston, Illinois 60208, United States;* orcid.org/0000-0003-4416-638X

Matthew L. Whitaker − *Mineral Physics Institute, Department of Geosciences, Stony Brook University, Stony Brook, New York 11794, United States; National Synchrotron Light Source II, Brookhaven National Laboratory, Upton, New York 11973, United States*

Tony Yu − *GeoSoilEnviroCARS, Center for Advanced Radiation Sources, The University of Chicago, Chicago, Illinois 60637, United States*

Gilberto Fabbris − *Advanced Photon Source, Argonne National Laboratory, Lemont, Illinois 60439, United States;* orcid.org/0000-0001-8278-4985

Yue Meng − *HPCAT, X-ray Science Division, Argonne National Laboratory, Argonne, Illinois 60439, United States*

Daniel Haskel − *Advanced Photon Source, Argonne National Laboratory, Lemont, Illinois 60439, United States*

Yanbin Wang − *GeoSoilEnviroCARS, Center for Advanced Radiation Sources, The University of Chicago, Chicago, Illinois 60637, United States;* orcid.org/0000-0001-5716-3183

Steven D. Jacobsen − *Department of Earth and Planetary Sciences, Northwestern University, Evanston, Illinois 60208, United States;* orcid.org/0000-0002-9746-958X

Complete contact information is available at: https://pubs.acs.org/10.1021/jacs.2c03485

Author Contributions

[⊥]A.D.T. and A.B.A. contributed equally.

Notes

The authors declare no competing financial interest.

■ ACKNOWLEDGMENTS

The authors would like to thank Dr. James P. S. Walsh, Dr. Doug Fabini, Dr. Ryan A. Klein, Dr. Lei Sun, Dr. Chung-Jui Yu, Dr. Stephen von Kugelgen, and Dr. Michael K. Wojnar for helpful discussions, and Dr. Chung-Jui Yu for assistance with the table of contents graphic. Experimental work was supported by the AFOSR (FA9550-17-1-0247). S.D.J. acknowledges support from the NSF (DMR-1508577) and beamtime provided through the Chicago/DOE Alliance Center. A.B.A. acknowledges support from the IIN Postdoctoral Fellowship and the Northwestern University International Institute of Nanotechnology. The multianvil cell assemblies used were from the COMPRES Cell Assembly Project, which was supported by COMPRES under NSF Cooperative Agreement EAR 1661511. This research used resources at XPD (sector 28) of the National Synchrotron Light Source II, a U.S. Department of Energy (DOE) Office of Science User Facility operated for the DOE Office of Science by Brookhaven National Laboratory under Contract No. DE-SC0012704. Use of the MAXPD Endstation was supported by COMPRES, the Consortium for Materials Properties Research in Earth Sciences, under NSF Cooperative Agreement No. EAR 16-61511, and by the Mineral Physics Institute, Department of Geosciences, Stony Brook University. A portion of this work was performed at GeoSoilEnviroCARS (Sector 13), Advanced Photon Source (APS), Argonne National Laboratory (ANL). GeoSoilEnviroCARS is supported by the National Science Foundation-Earth Sciences (EAR 0217473), Department of Energy−Geosciences (DE-FG02-94ER14466) and the State of Illinois. A portion of this work was performed at HPCAT (Sector 16), APS, ANL. HPCAT operations are supported by DOE-NNSA's Office of Experimental Sciences. The APS is a Department of Energy (DOE) Office of Science User Facility operated for the DOE Office of Science by ANL under Contract No. DE-AC02-06CH11357. M.J.W. and J.M.R. acknowledge support from the National Science Foundation (NSF) under Award Number DMR-2011208. Calculations were performed using the Center for Nanoscale Materials (Carbon) Cluster, an Office of Science user facility supported by the U.S. Department of Energy, Office of Science, Office of Basic Energy Sciences, under Contract No. DE-AC02-06CH11357 and the National Energy Research Scientific Computing Center (NERSC), a U.S. DOE Office of Science User Facility located at Lawrence Berkeley National Laboratory, operated under Contract No. DE-AC02-05CH11231. This work made use of the EPIC facility of the NUANCE Center, and IMSERC, which is supported by Soft and Hybrid Nanotechnology Experimental (SHyNE) Resource (NSFECCS-2025633); the MRSEC program (NSF DMR-1720139) at the Materials Research Center; the International Institute for Nanotechnology (IIN); the Keck Foundation; and the State of Illinois, through the IIN.

■ ABBREVIATIONS

MAP, multianvil press; MAXPD, Multi-Anvil X-ray Powder Diffraction; PXRD, powder X-ray diffraction; SOC, spin−orbit coupling; XAS, X-ray absorption spectroscopy

■ REFERENCES

(1) Narang, P.; Garcia, C. A. C.; Felser, C. The topology of electronic band structures. *Nat. Mater.* **2021**, *20*, 293−300.

(2) Kumar, N.; Guin, S. N.; Manna, K.; Shekhar, C.; Felser, C. Topological Quantum Materials from the Viewpoint of Chemistry. *Chem. Rev.* **2021**, *121* (5), 2780−2815.

(3) Sato, M.; Ando, Y. Topological superconductors: a review. *Rep. Prog. Phys.* **2017**, *80*, No. 076501.

(4) Yan, B.; Felser, C. Topological materials: Weyl semimetals. *Annu. Rev. Condens. Matter. Phys.* **2017**, *8*, 337−354.

(5) Yan, B.; Zhang, S.-C. Topological materials. *Rep. Prog. Phys.* **2012**, *75* (9), No. 096501.

(6) Barreto, L.; Kühnemund, L.; Edler, F.; Tegenkamp, C.; Mi, J.; Bremholm, M.; Iversen, B. B.; Frydendahl, C.; Bianchi, M.; Hofmann,

P. Surface-Dominated Transport on a Bulk Topological Insulator. *Nano Lett.* **2014**, *14*, 3755−3760.
(7) Ren, Z.; Taskin, A. A.; Sasaki, S.; Segawa, K.; Ando, Y. Large Bulk Resistivity and Surface Quantum Oscillations in the Topological Insulator Bi_2Te_2Se. *Phys. Rev. B* **2010**, *82*, 241306.
(8) Bansal, N.; Kim, Y. S.; Brahlek, M.; Edrey, E.; Oh, S. Thickness-Independent Transport Channels in Topological Insulator Bi_2Se_3 Thin Films. *Phys. Rev. Lett.* **2012**, *109* (11), 116804.
(9) Luo, L.; Cheng, D.; Song, B.; Wang, L.-L.; Vaswani, C.; Lozano, P. M.; Gu, G.; Huang, C.; Kim, R. H. J.; Liu, Z.; Park, J.-M.; Yao, Y.; Ho, K.; Perakis, I. E.; Li, Q.; Wang, J. A Light-Induced Phononic Symmetry Switch and Giant Dissipationless Topological Photocurrent in $ZrTe_5$. *Nat. Mater.* **2021**, *20*, 329−334.
(10) Sabzalipour, A.; Mir, M.; Zarenia, M.; Partoens, B. Two Distinctive Regimes in the Charge Transport of a Magnetic Topological Ultra Thin Film. *New J. Phys.* **2020**, *22*, 123004.
(11) He, Q. L.; Hughes, T. L.; Armitage, N. P.; Tokura, Y.; Wang, K. L. Topological Spintronics and Magnetoelectronics. *Nat. Mater.* **2022**, *21*, 15−23.
(12) Šmejkal, L.; Mokrousov, Y.; Yan, B.; MacDonald, A. H. Topological Antiferromagnetic Spintronics. *Nat. Phys.* **2018**, *14*, 242−251.
(13) Bonderson, P.; Sarma, S. D.; Freedman, M.; Nayak, C. A Blueprint for a Topologically Fault-Tolerant Quantum Computer. *arXiv (quant-ph)* March 15, 2010, 1003.2856, Ver 1. https://arxiv.org/abs/1003.2856 (accessed January 14, 2022).
(14) Nayak, C.; Simon, S. H.; Stern, A.; Freedman, M.; Das Sarma, S. Non-abelian anyons and topological quantum computation. *Rev. Mod. Phys.* **2008**, *80*, 1083−1159.
(15) Sau, J. D.; Tewari, S.; Das Sarma, S. Universal quantum computation in a semiconductor quantum wire network. *Phys. Rev. A* **2010**, *82*, No. 052322.
(16) Vijay, S.; Hsieh, T. H.; Fu, L. Majorana fermion surface code for universal quantum computation. *Phys. Rev. X.* **2015**, *5*, No. 041038.
(17) Vergniory, M. G.; Elcoro, L.; Felser, C.; Regnault, N.; Bernevig, B. A.; Wang, Z. A complete catalogue of high-quality topological materials. *Nature* **2019**, *566*, 480−485.
(18) Schoop, L. M.; Pielnhofer, F.; Lotsch, B. V. Chemical principles of topological semimetals. *Chem. Mater.* **2018**, *30*, 3155−3176.
(19) Fu, L. Topological Crystalline Insulators. *Phys. Rev. Lett.* **2011**, *106*, 106802.
(20) Cava, R. J.; Ji, H.; Fuccillo, M. K.; Gibson, Q. D.; Hor, Y. S. Crystal structure and chemistry of topological insulators. *J. Mater. Chem. C* **2013**, *1*, 3176−3189.
(21) Klemenz, S.; Hay, A. K.; Teicher, S. M. L.; Topp, A.; Cano, J.; Schoop, L. M. The Role of Delocalized Chemical Bonding in Square-Net-Based Topological Semimetals. *J. Am. Chem. Soc.* **2020**, *142*, 6350−6359.
(22) Badding, J. V. High-pressure synthesis, characterization, and tuning of solid-state materials. *Annu. Rev. Mater. Sci.* **1998**, *28*, 631−658.
(23) Zhang, L.; Wang, Y.; Lv, J.; Ma, Y. Materials discovery at high pressures. *Nat. Rev. Mater.* **2017**, *2*, 17005.
(24) Brazhkin, V. V. High-pressure synthesized materials: Treasures and hints. *High Press. Res.* **2007**, *27*, 333−351.
(25) Grochala, W.; Hoffmann, R.; Feng, J.; Ashcroft, N. W. The chemical imagination at work in very tight places. *Angew. Chem., Int. Ed.* **2007**, *46*, 3620−3642.
(26) Miao, M.; Sun, Y.; Zurek, E.; Lin, H. Chemistry under high pressure. *Nat. Rev. Chem.* **2020**, *4*, 508−527.
(27) Rahm, M.; Cammi, R.; Ashcroft, N. W.; Hoffmann, R. Squeezing All Elements in the Periodic Table: Electron Configuration and Electronegativity of the Atoms Under Compression. *J. Am. Chem. Soc.* **2019**, *141*, 10253−10271.
(28) Tencé, S.; Janson, O.; Krellner, C.; Rosner, H.; Schwarz, U.; Grin, Y.; Steglich, F. $CoBi_3$− the First Binary Compound of Cobalt with Bismuth: High-pressure Synthesis and Superconductivity. *J. Phys.: Condens. Matter* **2014**, *26*, 395701.
(29) Walsh, J. P. S.; Clarke, S. M.; Meng, Y.; Jacobsen, S. D.; Freedman, D. E. Discovery of $FeBi_2$. *ACS Cent. Sci.* **2016**, *2*, 867−871.
(30) Clarke, S. M.; Walsh, J. P. S.; Amsler, M.; Malliakas, C. D.; Yu, T.; Goedecker, S.; Wang, Y.; Wolverton, C.; Freedman, D. E. Discovery of a Superconducting Cu−Bi Intermetallic Compound by High-Pressure Synthesis. *Angew. Chem., Int. Ed.* **2016**, *55*, 13446−13449.
(31) Altman, A. B.; Tamerius, A. D.; Koocher, N. Z.; Meng, Y.; Pickard, C. J.; Walsh, J. P. S.; Rondinelli, J. M.; Jacobsen, S. D.; Freedman, D. E. Computationally Directed Discovery of $MoBi_2$. *J. Am. Chem. Soc.* **2021**, *143*, 214−222.
(32) Lee, H.; Yazyev, O. V. Interplay between Spin−Orbit Coupling and Crystal-Field Effect in Topological Insulators. *J. Phys.: Condens. Matter* **2015**, *27*, 285801.
(33) Sheng, X.-L.; Wang, Z.; Yu, R.; Weng, H.; Fang, Z.; Dai, X. Topological Insulator to Dirac Semimetal Transition Driven by Sign Change of Spin-Orbit Coupling in Thallium Nitride. *Phys. Rev. B* **2014**, *90*, 245308.
(34) Nash, P. The Ni−Pb (nickel−lead) system. *Bull. Alloy Phase Diagr.* **1987**, *8*, 264−301.
(35) Kainulainen, I.; Taskinen, P.; Gisby, J. A thermodynamic assessment of the nickel−lead system. *CALPHAD* **2010**, *34*, 441−445.
(36) Ritti, R. R.; Diximier, J.; Guinier, A. Formation de la phase NiPb par evaporations simultanees du nickel et du plomb. *C. R. Acad. Sc. Paris* **1968**, *266*, 565−567.
(37) De Marcillac, P.; Coron, N.; Dambier, G.; Leblanc, J.; Moalic, J.-P. Experimental Detection of α-particles from the radioactive decay of natural bismuth. *Nature* **2003**, *422*, 876−878.
(38) Verstraete, M. J.; Torrent, M.; Jollet, F.; Zérah, G.; Gonze, X. Density functional perturbation theory with spin-orbit coupling: Phonon band structure of lead. *Phys. Rev. B* **2008**, *78*, No. 045119.
(39) Smirnov, N. A. Effect of spin-orbit interactions on the structural stability, thermodynamic properties, and transport properties of lead under pressure. *Phys. Rev. B* **2018**, *97*, No. 094114.
(40) Leinenweber, K. D.; Tyburczy, J. A.; Sharp, T. G.; Soignard, E.; Diedrich, T.; Petuskey, W. B.; Wang, Y.; Mosenfelder, J. L. Cell assemblies for reproducible multi-anvil experiments (the COMPRES assemblies). *Am. Mineral.* **2012**, *97*, 353.
(41) Coelho, A. A. *TOPAS Academic: General Profile and Structure Analysis Software for Powder Diffraction Data;* Bruker AXS: Karlsruhe, Germany, 2007.
(42) Fjellvåg, H.; Kjekshus, A. Structural Properties of Co_3Sn_2, Ni_3Sn_2 and some ternary derivatives. *Acta Chem. Scand.* **1986**, *40a*, 23−30.
(43) Lidin, S.; Larsson, A. K. A Survey of Superstructures in Intermetallic NiAs-Ni2In-Type Phases. *J. Solid State Chem.* **1995**, *118*, 313−322.
(44) Pauling, L. Atomic Radii and Interatomic Distances in Metals. *J. Am. Chem. Soc.* **1947**, *69* (3), 542−553.
(45) Walsh, J.; Clarke, S. M.; Puggioni, D.; Tamerius, A. D.; Meng, Y.; Rondinelli, J. M.; Jacobsen, S. D.; Freedman, D. E. $MnBi_2$: A Metastable High-Pressure Phase in the Mn−Bi System. *Chem. Mater.* **2019**, *31*, 3083−3088.
(46) Tamerius, A. D.; Clarke, S. M.; Gu, M.; Walsh, J. P. S.; Esters, M.; Meng, Y.; Hendon, C. H.; Rondinelli, J. M.; Jacobsen, S. D.; Freedman, D. E. Discovery of Cu_3Pb. *Angew. Chem. Int. Ed.* **2018**, *57*, 12809−12813.
(47) Perdew, J. P.; Burke, K.; Ernzerhof, M. Generalized Gradient Approximation Made Simple. *Phys. Rev. Lett.* **1996**, *77*, 3865.
(48) Vergniory, M. G.; Wieder, B. J.; Elcoro, L.; Parkin, S. S. P.; Felser, C.; Bernevig, B. A.; Regnault, N. All Topological Bands of All Stoichiometric Materials. *arXiv (cond-mat.mtrl-sci)* May 20, **2021**, 2105.09954, Ver. 1. https://arxiv.org/abs/2105.09954 (accessed May 20, 2022).
(49) Hu, Y.; Yue, C.; Yuan, D.; Gao, J.; Huang, Z.; Fang, Z.; Fang, C.; Weng, H.; Zhang, W. The Evolution of Weyl Nodes in Ni Doped Thallium Niobate Pyrochlore $Tl_{2-x}Ni_xNb_2O_7$. *arXiv (cond-mat.mtrl-sci)* December 8, **2021**, 2112.04127, Ver. 1. https://arxiv.orgabs/2112.04127 (accessed June 7, 2022).

https://doi.org/10.1021/jacs.2c03485
J. Am. Chem. Soc. XXXX, XXX, XXX−XXX

(50) Sarkar, A. B.; Mardanya, S.; Huang, S.-M.; Ghosh, B.; Huang, C.-Y.; Lin, H.; Bansil, A.; Chang, T.-R.; Agarwal, A.; Singh, B. Magnetically Tunable Dirac and Weyl Fermions in the Zintl Materials Family. *Phys. Rev. Mater.* **2022**, *6*, No. 044204.
(51) Xu, Y.; Song, Z.; Wang, Z.; Weng, H.; Dai, X. Higher-Order Topology of the Axion Insulator $EuIn_2As_2$. *Phys. Rev. Lett.* **2019**, *122*, 256402.
(52) da Silva, E. L.; Leonardo, A.; Yang, T.; Santos, M. C.; Vilaplana, R.; Gallego-Parra, S.; Bergara, A.; Manjón, F. J. β-As_2Te_3: Pressure-Induced Three-Dimensional Dirac Semimetal with Ultralow Room-Pressure Lattice Thermal Conductivity. *Phys. Rev. B* **2021**, *104*, No. 024103.
(53) Tanaka, Y.; Takahashi, R.; Zhang, T.; Murakami, S. Theory of Inversion-Z_4 Protected Topological Chiral Hinge States and Its Applications to Layered Antiferromagnets. *Phys. Rev. Res.* **2020**, *2*, No. 043274.
(54) Bradlyn, B.; Elcoro, L.; Cano, J.; Vergniory, M. G.; Wang, Z.; Felser, C.; Aroyo, M. I.; Bernevig, B. A. Topological quantum chemistry. *Nature* **2017**, *547*, 298−305.
(55) *Topological Materials Database, Predicted electronic band structure*; NiAs ICSD-5245. Topological Materials Database https://www.topologicalquantumchemistry.org/#/detail/5245 (accessed November 15, 2021).
(56) *Topological Materials Database, Predicted electronic band structure*; Ni_2In ICSD-62017. Topological Materials Database https://www.topologicalquantumchemistry.org/#/detail/62017 (accessed November 15, 2021).
(57) *Bilbao Crystallographic Server*. https://www.cryst.ehu.es/ (accessed November 15, 2021).
(58) *Topological Materials Database, Predicted electronic band structure*; Ni_3Sn_2 ICSD-105358. Topological Materials Database https://www.topologicalquantumchemistry.org/#/detail/105358 (accessed November 15, 2021).
(59) Jandl, I.; Ipser, H.; Richter, K. W. Thermodynamic modelling of the general NiAs-type structure: A study of first principle energies. *CALPHAD* **2015**, *50*, 174−181.
(60) Bearden, J. A.; Burr, A. F. Reevaluation of X-ray Atomic Energy Levels. *Rev. Mod. Phys.* **1967**, *39*, 125−142.
(61) Li, C.; Chen, Y.; Zhang, S.; Xu, S.; Zhou, J.; Wang, F.; Wei, M.; Evans, D. G.; Duan, X. Ni−In Intermetallic Nanocrystals as Efficient Catalysts toward Unsaturated Aldehydes Hydrogenation. *Chem. Mater.* **2013**, *25*, 3888−3896.
(62) Marakatti, V. S.; Arora, N.; Rai, S.; Sarma, S. Ch.; Peter, S. C. Understanding the Role of Atomic Ordering in the Crystal Structures of Ni_xSn_y toward Efficient Vapor Phase Furfural Hydrogenation. *ACS Sustain. Chem. Eng.* **2018**, *6*, 7325−7338.
(63) Onda, A.; Komatsu, T.; Yashima, T. Characterizations and catalytic properties of fine particles of Ni−Sn intermetallic compounds supported on SiO_2. *J. Catal.* **2004**, *221*, 378−385.
(64) Fawcett, S. E.; Gordon, R. A.; Jamieson, H. E. Optimizing experimental design, overcoming challenges, and gaining valuable information from the Sb K-edge XANES region. *Am. Mineral.* **2009**, *94*, 1377−1387.
(65) Sham, T. K. X-ray Absorption studies of unoccupied d-band states in gold and nickel metallic compounds. *Solid State Commun.* **1987**, *64*, 1103−1106.

https://doi.org/10.1021/jacs.2c03485
J. Am. Chem. Soc. XXXX, XXX, XXX−XXX